High-energy aqueous magnesium ion batteries with capacity-compensation evolved from dynamic copper ion redox

*Shuxin Zhang, Yaowei Wang, Yukun Sun, Yaru Wang, Yang Yang, Peng Zhang, Xuecheng Lv, Jiulin Wang, Hong Zhu, Yanna NuLi**

S. X. Zhang, Y. K. Sun, Y. R. Wang, Dr. Y. Yang, P. Zhang, Prof. J. L. Wang, and Prof. Y. N. NuLi

School of Chemistry and Chemical Engineering, Shanghai Electrochemical Energy Devices Research Center, Shanghai Jiao Tong University, Shanghai 200240, P. R. China

E-mail: nlyn@sjtu.edu.cn

Y. W. Wang, Prof. H. Zhu

University of Michigan-Shanghai Jiao Tong University Joint Institute, Shanghai Jiao Tong University, Shanghai 200240, P. R. China

X. C. Lv

School of Energy and Power Engineering, Dalian University of Technology, Dalian, 116024, P.R. China

Keywords: magnesium ion batteries, aqueous electrolyte, high energy density, capacity-compensation, copper

Abstract: The low specific capacity and low voltage plateau are significant challenges in the advancement of practical magnesium ion batteries (MIBs). Here, a superior aqueous

This is the author manuscript accepted for publication and has undergone full peer review but has not been through the copyediting, typesetting, pagination and proofreading process, which may lead to differences between this version and the Version of Record. Please cite this article as doi: 10.1002/smll.202300148.

This article is protected by copyright. All rights reserved.

Author Manuscript

electrolyte combining with a copper foam interlayer between anode and separator is proposed to address these drawbacks. Notably, with the dynamic redox of copper ions, the weakened solvation of Mg^{2+} cations in the electrolyte and the enhanced electronic conductivity of anode, which may offer effective capacity-compensation to the PTCDI-Mg conversion reactions during the long-term cycles. As a result, the unique MIBs using expanded graphite (EG) cathode coupled with 3,4,9,10-perylenetetracarboxylic diimide (PTCDI) anode demonstrate exceptional performance with an ultra-high capacity (205 mAh g^{-1}, 243 Wh kg^{-1} at 5 A g^{-1}) as well as excellent cycling stability after 600 cycles and rate capability (138 mAh g^{-1}, 81 Wh kg^{-1} at 10 A g^{-1}).

1. Introduction

Owing to the long cycle life, high cycling efficiency and large energy density, lithium-ion batteries (LIBs) have triggered worldwide interest and been widely used for portable devices and electric vehicles during the past decades [1]. Unfortunately, the prices of lithium salts have been increasing and recently exerted considerable pressure on the market [2], and the limited crustal abundance of Li, Ni and Co used for cathode materials cannot fulfill the boosting market needs [3]. Besides, safety concerns regarding flammable electrolytes and thermal runaway have made them difficult to alleviate public concerns [4]. Given these challenges, the development of low-cost and safe battery systems has become increasingly crucial and desirable [5]. Recent years, multivalent ion (e.g., Mg^{2+} [6], Ca^{2+} [7], Al^{3+} [8]) batteries have been considered as promising alternatives to LIBs, because they have the

This article is protected by copyright. All rights reserved.

Author Manuscript

potential to achieve higher theoretical energy densities than monovalent ion batteries. Among them, rechargeable magnesium batteries (RMBs) with Mg anode are particularly attractive due to the high volumetric energy density (3833 mAh cm^{-3}), which is approximately twice that of lithium (2062 mAh cm^{-3}) [9]. Additionally, Mg is one of the most abundant elements on earth (8th in the earth's crust and 3rd in seawater). Although great effort has been devoted over the past decades, RMBs still suffer from two major challenges: i) the easy passivation of metal Mg anode, which makes it difficult to achieve a high Coulombic efficiency for magnesium electrolytes. While various types of specially designed Mg compatible electrolytes have been introduced to achieve reversible Mg plating-stripping [10], a steep cost, environmental harm and low levels of anodic stability limit their broader application. Fortunately, this problem does not exist in magnesium ion batteries (MIBs) without magnesium metal; ii) the strong Coulombic interaction between the host materials and Mg^{2+} ions, which results in slow solid-state Mg^{2+} diffusions and large polarization effect, as well as low Mg^{2+} intercalation levels and rapid capacity decay [11]. The slow Mg^{2+} diffusion can be alleviated by implementing partially crystalline/amorphous organic cathodes, where the conformational flexibility of polymeric chains can facilitate Mg^{2+} diffusion [12]. On the other hand, the dual-ion batteries (DIBs) could be another effective approach to address this issue.

Unlike conventional batteries based on the shuttling back and forth of the same cations between the cathode and anode during charge-discharge cycles, DIBs allow both cations and anions to insert/de-insert into electrodes upon cycling [13]. Specifically, the cations insert into the anode while the anions synchronously insert into the cathode during charging and vice

This article is protected by copyright. All rights reserved.

Author Manuscript

versa. In DIBs, the ion diffusion kinetics could be improved due to the reduced diffusion distance. Besides, the working voltage can be increased (>4.5 V vs. Li/Li^+) and the cost can be decreased by using inexpensive graphite material of inserting anions as the cathode of DIBs. Particularly, Mg-ion-based DIBs (Mg-DIBs) that use a graphite cathode and an organic anode to accommodate ions could combine the benefits of MIBs and DIBs, and achieve high-rate capability and good stability. A Mg-DIB with 0.1 mol L^{-1} magnesium trifluoromethanesulfonate ($Mg(OTf)_2$) in 1-butyl-3-methyl-imidazolium hexafluorophosphate ($BMIMPF_6$) ionic liquid obtained a capacity of 51 mAh g^{-1} and 62% Coulombic efficiency after 60 cycles [14]. The coupling of graphite cathode and $TiNb_2O_5$ anode with the electrolyte of magnesium bis(trifluoromethanesulfonyl)imid ($Mg(TFSI)_2$) in 1-butyl-1-methylpyrrolidinium bis(trifluoromethanesulfonyl)imide ($Pyr_{14}TFSI$) can realize 60 mAh g^{-1} at 3C during 500 cycles [15]. An organic Mg-DIB using polytriphenylamine (PTPAn) as the cathode, perylene diimide-ethylene diamine (PDI-EDA) as the anode and an anhydrous acetonitrile (AN) solution of magnesium perchlorate ($Mg(ClO_4)_2$ as the electrolyte exhibits 73 mAh g^{-1} capacity at a high current density of 1 A g^{-1} [16]. Recently, a Mg-DIB with a redox polymer (poly(vinyl carbazole), PVCz) cathode and an alloy-type ($3Mg/Mg_2Sn$) anode in $Mg(TFSI)_2$/AN electrolyte was proposed, demonstrating 122 mAh g^{-1} discharge capacity and the unprecedented high energy density (384 Wh kg^{-1}) and power density (6300 W kg^{-1}) at 1.5 A g^{-1} [12]. Despite these great advancements, few of these strategies have brought about a near-practical improvement, especially because the obtained specific capacities are still much

Author Manuscript

This article is protected by copyright. All rights reserved.

lower than practical standard, and the use of organic electrolytes could increase the battery cost and cause the safety problem.

Aqueous electrolytes have more advantages than organic electrolytes, such as higher safety, better environmental friendliness, lower cost, higher ionic conductivity and faster ion diffusion kinetics [17]. However, the relatively low charging cut-off voltage (<1.80 V) of aqueous electrolytes leads to low specific capacities. Aqueous/organic hybrid electrolytes inherit a fast dynamic and a wide voltage window from aqueous and organic electrolytes, respectively. The small amount of water introduced into the organic electrolytes could "shield" the charges of divalent Mg^{2+} ions and promote reversible Mg^{2+} insertion/deinsertion, consequently improving cycling stability and rate capability [18]. It has been reported that Cu current collector or Cu interlayer was used to modify the electrochemical performance of Mg-S (Mg-Se) batteries [19]. Formed sulfides (selenides) and the interaction between the Cu metal and magnesium polysulfides (polyselenides) play critical roles to the markedly improved reaction kinetics [19d, 20]. However, there were no relevant reports on the key role of Cu element in MIBs and Mg-DIBs.

In this study, we develop a Mg-DIB containing a graphite cathode coupled with a 3,4,9,10-perylenetetracarboxylic diimide (PTCDI) anode and a novel hybrid aqueous/organic electrolyte (1 mol L^{-1} $Mg(TFSI)_2$ in deionized water and acetonitrile (AN)) with a Cu foam interlayer between anode and separator, as shown in Figure 1a. The unusual Mg-DIBs take the advantage of organic and aqueous solvent components such as a wide electrochemical window (Figure 1b) and fast ion diffusion kinetics, exhibiting high working voltage and rate

This article is protected by copyright. All rights reserved.

Author Manuscript

capability, and a remarkable cycling stability. In addition, it was confirmed that Cu foam interlayer undergoes two consecutive redox steps: Cu(0)↔Cu(I), Cu(I)↔Cu(II), which offers effective capacity-compensation to the PTCDI-Mg conversion reactions. Moreover, the calculated results demonstrate that the existence of Cu^{2+} cations significantly reduces the interaction of Mg^{2+} cations with the solvent molecules and $TFSI^-$, making Mg^{2+} cations to react with PTCDI more easily. Furthermore, in-situ formation of metal Cu on the PTCDI anode improves the electronic conductivity of the organic anode, thus accelerates the promotion of the rate capability and long-term durability of the full cell. This innovative strategy opens a door for the practical application of rechargeable magnesium ion batteries with excellent electrochemical performance.

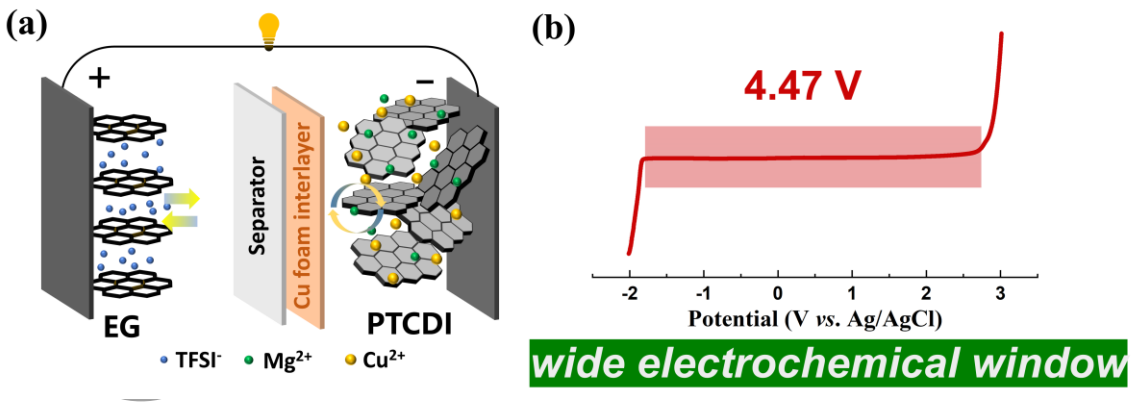

Figure 1. (a) Mg-DIB structure containing Cu foam interlayer; (b) LSV curve showing the electrochemical window of the hybrid aqueous/organic electrolyte.

2. Results and Discussion

The hybrid electrolyte of 1 mol L^{-1} $Mg(TFSI)_2$ in AN/H_2O at a 4.9:0.1 volume ratio displays a 4.47 V electrochemical window from -1.8 V to 2.6 V *vs* Ag/AgCl (Figure 1b),

This article is protected by copyright. All rights reserved.

Author Manuscript

which is wider than those with other AN/H_2O ratios (such as 4.7:0.3, 4.5:0.5 and 4.0:1.0, Figure S1). If not specially stated, the volume ratio of AN/H_2O in the hybrid electrolyte is 4.9:0.1 in this work. Such an electrochemical window is significantly wider than that of the aqueous electrolyte (2.05 V) and close to that of organic solution (5.23 V), as shown in Figure S2. The electrochemical stabilization window of 4.47 V creates promising opportunities for improving the energy density of the full batteries. Compared with the organic and aqueous electrolytes (Figure S3), the hybrid electrolyte delivers an ionic conductivity of 2.18 mS cm^{-1}, which is higher than the organic electrolyte (2.08 mS cm^{-1}) and close to the aqueous electrolyte (2.21 mS cm^{-1}), contributing the potential to obtain fast electrochemical kinetics.

Author Manuscript

This article is protected by copyright. All rights reserved.

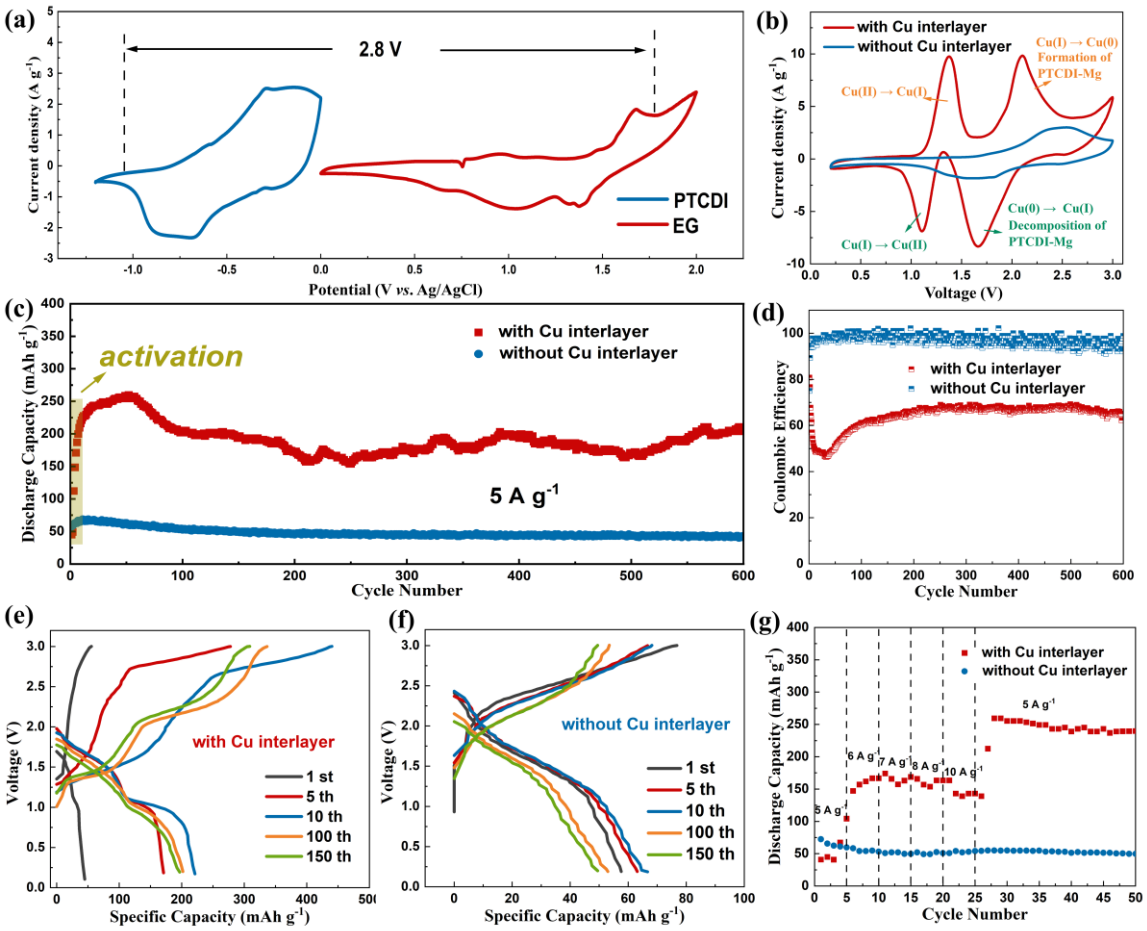

Figure 2. (a) CV curves for the 3rd cycle of PTCDI and EG electrodes at 5 mV s^{-1} in a three-electrode system; (b) Typical CV curves of EG||PTCDI full cells with and without Cu foam interlayer at 5 mV s^{-1}; (c) Cycling performance of the full cells with and without Cu foam interlayer at a current density of 5 A g^{-1}; (d) Coulombic efficiency of the full cells with and without Cu foam interlayer; Discharge-charge curves of the full cells during 150 cycles with Cu foam interlayer (e) and without Cu foam interlayer (f) at 5 A g^{-1}; (g) Rate capability of full cells with and without Cu foam interlayer from the current density of 5 A g^{-1} to 10 A g^{-1}.

Author

This article is protected by copyright. All rights reserved.

Cyclic voltammetry (CV) measurements of the PTCDI and EG electrodes in the $Mg(TFSI)_2$ electrolyte were carried out at a scan rate of 5 mV s^{-1} in the voltage range of -1.2~0.0 V and 0.0~2.0 V, respectively, with PTCDI or EG as the working electrode, platinum as the counter electrode, and standard Ag/AgCl electrode as the reference electrode (the 3rd cycle in Figure 2a, and the complete cycles in Figure S4 and S5). For PTCDI electrode, two reduction peaks around -0.68 V and -0.84 V corresponding to the reduction of the C=O groups in PTCDI forming PTCDI-Mg are observed, together with two oxidation peaks around -0.29 V and -0.12 V that originate from the oxidation of PTCDI-Mg to revert to C=O groups. Different from the typical intercalation/deintercalation curve of cations into graphite [21], the CV curve of EG electrode proves the insertion/deinsertion of $TFSI^-$ anions in graphite, similar to the behaviors of other anions (PF_6^-, Otf^-) [14, 22].

The electrochemical performance of the Mg-DIBs full cell with EG cathode and PTCDI anode was further evaluated. When the potential exceeds 1.8 V (*vs*. Ag/AgCl), the EG electrode would be oxidated to form CO_2 [23]. The cut-off voltage range of the full cell was set at 0.2~3.0 V considering the 2.8 V electrochemical window (marked in Figure 2a) between the EG cathode and the PTCDI anode. Because the mass loading of EG cathode is much larger than that of PTCDI anode (ca. 10:1), the electrochemical properties of the full cell mainly depend on that of PTCDI anode. Figure 2b shows the CV curves of the Mg-DIB full cell in the $Mg(TFSI)_2$ electrolyte with or without Cu foam interlayer at a scan rate of 5 mV s^{-1} in the voltage range of 0.2~3.0 V. Apparently, differing from that without Cu foam interlayer only having a couple of cathodic/anodic peak at approximately 1.71 V/2.53 V, the curve with

This article is protected by copyright. All rights reserved.

Author Manuscript

Cu foam interlayer exhibits two sharpening peaks at approximately 1.67 V/2.09 V and 1.09 V/1.38 V during cycles, which could be assigned to the redox of Cu(0) ↔ Cu(I), and the reversible reaction of Mg^{2+} with PTCDI as well as the redox of Cu(I) ↔ Cu(II), respectively.

The cycling performance of Mg-DIB with or without Cu foam interlayer in the $Mg(TFSI)_2$ electrolyte is given in Figure 2c. When containing Cu foam interlayer, the cell is demonstrated to exhibit a reversible discharge capacity of around 205 mAh g^{-1} (243 Wh kg^{-1}) at 5 A g^{-1} in the voltage range of 0.2~3.0 V, much higher than that without Cu foam interlayer and conventional Mg-DIBs reported [12, 14-16, 24], and good cycling stability after 600 cycles. Due to the generation of Cu^{2+} cations from Cu interlayer in the first several cycles, the specific capacity of the cell gradually increases through a quick "activation" process, as shown in the highlighted area of Figure 2c. The half-battery cycling performance with PTCDI electrode and copper foam interlayer was further evaluated via a three-electrode cell with Pt counter electrode and Ag/AgCl reference electrode in Figure S6. The PTCDI electrode stabilized at around 210 mAh g^{-1} specific capacity at 5 A g^{-1}, illustrating the contribution of copper ions to the capacity of the full cell. Compared to the increased capacity with high Coulombic efficiency at low current densities for the full cell without Cu interlayer, the capacity and Coulombic efficiency of the full cell with Cu interlayer decrease significantly at a lower current of 1 A g^{-1} (Figure S7a), which is probably related to some parasitic reactions caused by the continuous dissolution of Cu interlayer at low current densities. High-rate conditions to a certain extent lead to a suppression by shortening their retention time before the transformation into the final products (Figure S7b). We also noticed that the Coulombic

This article is protected by copyright. All rights reserved.

Author Manuscript

efficiency of Mg-DIB with Cu foam interlayer is much lower than that without Cu (Figure 2d). The functional mechanism of Cu foam interlayer in this Mg-DIB system will be discussed in detail below. Figure 2e, f show the completely different charge-discharge curves at the 1st, 5th, 10th, 100th and 150th cycles for the Mg-DIB with or without Cu foam interlayer, respectively. The voltage plateaus of charge-discharge curves exactly fulfill the peaks of CVs. Compared to that without Cu foam interlayer, the charge curves after the 10th cycle exhibit a short additional voltage profile from 1.3 to 1.6 V and a longer voltage profile from 2.0 to 2.5 V for the cell with Cu foam interlayer, corresponding to the reduction of Cu^{2+} to Cu^{+} and the mixed reaction (C=O groups in PTCDI to PTCDI-Mg as well as Cu(I) to Cu(0)) at anode side, respectively. Correspondingly, the discharge curves show a sloping voltage profile from 1.7 to 1.45 V and a short voltage profile from 1.0 to 0.93 V, related to the mixed oxidation reaction (PTCDI-Mg to C=O groups as well as Cu(0)→Cu(I)) and Cu(I)→Cu(II) at anode side, respectively. Meanwhile, EG cathode experiences a reversible insertion/deinsertion of $TFSI^{-}$ during the charge/discharge process for the full cell with or without Cu foam interlayer. It also was notable that the "activation" process can be demonstrated in the Figure 2e. Dynamic copper ion redox gradually emerges and exhibits a voltage plateau, which plays as capacity-compensation species and subsequently delivers good repeatability profiles after 100 cycles. Figure 2g exhibits admirable rate capability with a capacity of 40.9, 156.9, 163.4, 143.0 and 138.9 mAh g^{-1} at the varied current density of 5, 6, 7, 8 and 10 A g^{-1} with Cu foam interlayer. When the current density returns to 5 A g^{-1}, the capacity achieves to 239.3 mAh g^{-1}, much greater than the initial capacity at the same current

Author Manuscript

This article is protected by copyright. All rights reserved.

density, further confirming gradual activation process triggered by copper ion redox. The excellent recover capability indicates its superior rate performance of the EG||PTCDI full cell with Cu foam interlayer. While the cell without the interlayer exhibits much lower capacity, suggesting PTCDI anode could be not enough to react with Mg^{2+} ions and has poor electronic conductivity. Moreover, rate performance test after fully activation with Cu foam interlayer was conducted as exhibited in Figure S8, the cell after fully activation with Cu foam interlayer still exhibits excellent rate performance.

To understand the two sharpening peaks related to the copper ions, we collect the CV results of full cell without Cu foam interlayer in $Cu(TFSI)_2$ electrolyte at a scan rate of 5 mV/s, as shown in Figure S9. It is quite interesting that there is no difference between the curves with or without PTCDI anode, confirming that copper ions do not react with the PTCDI. Moreover, the CV curves exhibit two pairs of widen cathodic/anodic peaks at 1.58 V/2.68 V and 0.93 V/1.62 V, which can be assigned with Cu(0) ↔ Cu(I) and Cu(I) ↔ Cu(II), respectively. It is notable that the area of the oxidation peak is much larger than that of the reduction peak, indicating that the charging capacity is much larger than the discharging capacity and thus a lower Coulombic efficiency is obtained. This could be attributed to the irreversibility of the redox process of copper ions. The cycling property of EG||PTCDI cells with $Cu(TFSI)_2$ electrolyte is given in Figure S10. The charging capacity of the first cycle is much larger than the discharging capacity, which proves the irreversibility of the redox process of copper ions, and the subsequent cycles are all in similarity (Figure S10a inset). The Coulombic efficiency is only about 20% during these cycles (Figure S10b). The low

This article is protected by copyright. All rights reserved.

Author Manuscript

Coulombic efficiency is due to the partial dissolution of metallic copper, which aligns with the prior report [25]. Possible solutions to enhance the Coulombic efficiency include altering the solvents, incorporating ionic liquids, or introducing additives in the electrolyte to adjust the deposition morphology of copper.

The detailed morphology and the element distribution of the PTCDI anode obtained after charging EG||PTCDI cell were examined by HAADF-STEM, as displayed in Figure 3a-c. The brighter parts in the anode (Figure 3a) are related to PTCDI material because of its higher conductivity in gold grid. The PTCDI anode after charging exhibits an irregular structure, in which C, O, N, Mg elements distribute evenly in the electrode (Figure 3b). Remarkably, Mg element enriches at the positions where the O, N elements are concentrated, which is associated with the formation of PTCDI-Mg through the Mg-O bonds. In order to prove the absence of Cu in the anode of the charged full cell, Cu element was added in the EDX mapping. It should be noted that we used gold grid to eliminate the influence of the carrier on the accuracy of EDX. As shown in Figure 3c, Cu element does not appear synchronously with any element of PTCDI, confirming that Cu hardly reacts with PTCDI active material. In addition, we primarily employed the first principles calculation to prove copper ions cannot react with PTCDI. Figure 3d presents the optimized four PTCDI-Cu structures in different cases, and the corresponding calculated formation energy values are depicted in Figure 3e, the detailed data for the optimization structures are summarized in Table S1. The formation energy is calculated by equation (1):

$$E_f = E_{PTCDI+nCu} - E_{PTCDI} - n \times E_{Cu} \quad (1)$$

This article is protected by copyright. All rights reserved.

Author Manuscript

where n is the number of Cu atoms combined with PTCDI crystal, $E_{PTCDI+nCu}$, E_{PTCDI} and E_{Cu} are the DFT energies of the PTCDI crystal with the insertion of n Cu atoms, PTCDI crystal and bulk Cu atoms, respectively. The optimized structs 1-4 are attached in Supplementary (separate file). When Cu ions are inserted into PTCDI, the calculation shows very high formation energy (> 0 eV), proving that the reaction is unlikely to occur. In the CV curves at various cycles of the EG||PTCDI full cell with Cu foam interlayer and $Mg(TFSI)_2$ electrolyte (Figure S11), the first cycle curve is a bit different from the others, which could be ascribed to the generation of PTCDI-Mg at the anode side in the first charging process; and the formation of PTCDI as well as Cu(0) → Cu(I) at around 1.65 V, Cu(I) → Cu(II) at around 1.10 V in the first discharging process. The intensity of all the redox peaks enhances with the increase of cycles, indicating that the material experiences an activation process stimulated by the generated copper ions upon cycling.

Author Manuscript

This article is protected by copyright. All rights reserved.

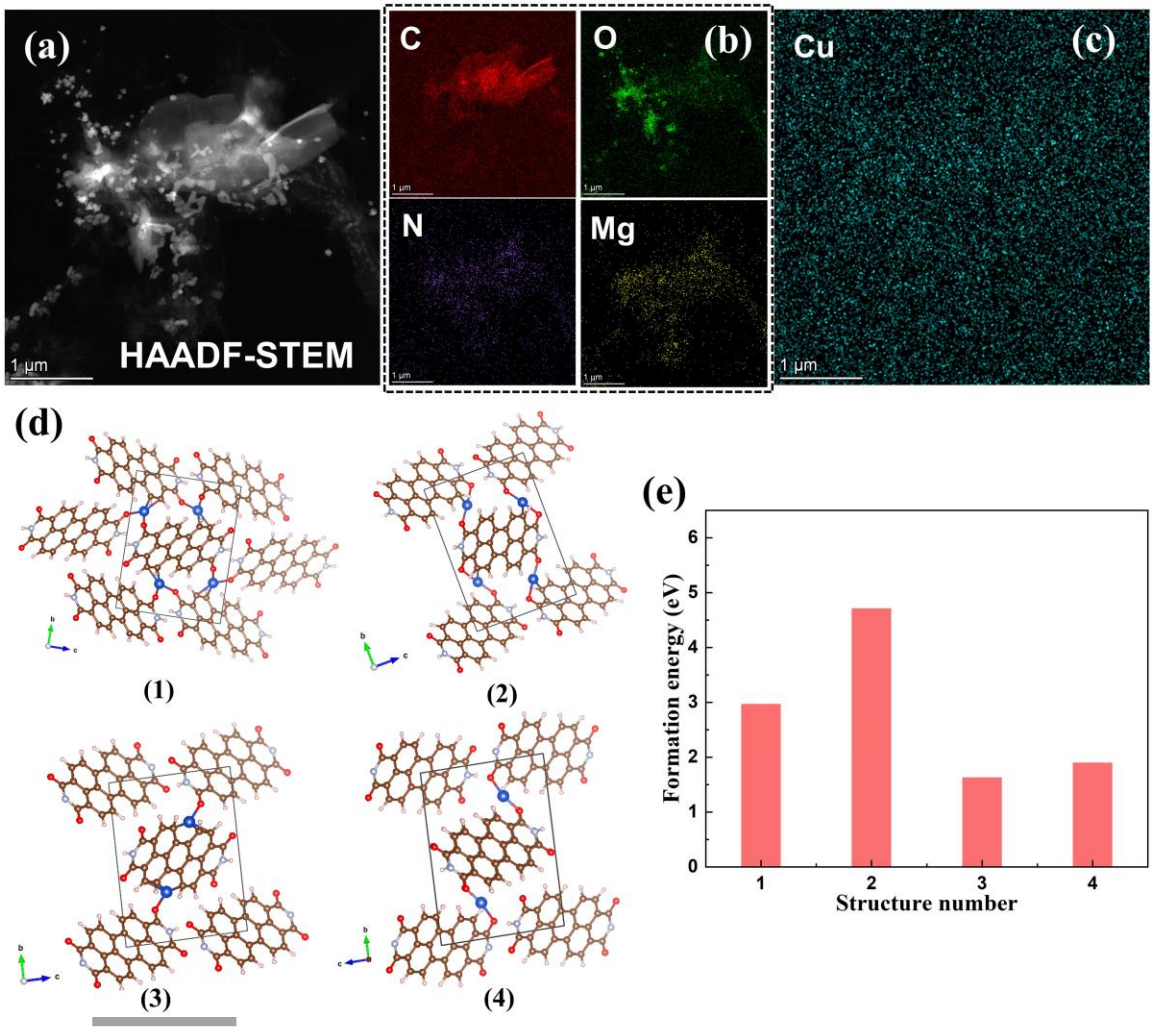

Figure 3. HAADF-STEM image (a), EDX mappings of C, O, N, Mg (b) and Cu (c) for the PTCDI electrode after fully charging the EG||PTCDI cell with Cu foam interlayer and $Mg(TFSI)_2$ electrolyte. (d) Unit cells of different PTCDI-Cu intercalation structures, the color codes for the atoms are as follows: blue, Cu; brown, C; red, O; gray, N and white, H; (e) The corresponding calculated formation energy of different PTCDI-Cu intercalation structures.

In order to verify the functional mechanism of Cu foam interlayer in this Mg-DIB system, the CV measurement of the Cu foam in the $Mg(TFSI)_2$ electrolyte was carried out at a scan rate of 5 mV s^{-1} in the voltage range of -2.0~3.0 V, with Cu foam as the working electrode,

Author

This article is protected by copyright. All rights reserved.

platinum as the counter electrode, and standard Ag/AgCl electrode as the reference electrode. As shown in Figure S12a, the solution turns light blue after the CV measurement, revealing that the Cu foam has experienced an electrochemical oxidation reaction to form Cu^{2+}, whose color is exactly the same as the color of the $Cu(TFSI)_2$ (Figure S12b). Thus, it can be concluded that Cu^{2+} ions are present in the form of $Cu(TFSI)_2$ after Cu foam is oxidized in the $Mg(TFSI)_2$ electrolyte. To eliminate the possibility that carbon paper current collector participates in the electrochemical reaction, carbon paper is alone used as the anode without PTCDI active material. The open circuit voltage of the full cell with EG cathode is around 0 V and remains little change after 2.5 h charging (Figure S13), demonstrating that the carbon paper hardly delivers any capacity. When Cu foil is directly used as the anode current collector without Cu foam interlayer, the EG||PTCDI full cell effectively works less than 30 cycles along with similar specific capacities but lower Coulombic efficiencies than that using Cu foam interlayer and carbon paper anode current collector (Figure S14a). We noticed that some floccule falls off from the PTCDI anode with the Cu foil current collector after the cycles. These floccule may be $Cu(TFSI)_2$ formed by the reaction of Cu current collector and the electrolyte via an electrochemical oxidation (Figure S14b), making PTCDI material exfoliates from the Cu current collector, thus it is impossible to achieve long cycles. Therefore, carbon paper anode current collector and Cu foam interlayer are more suitable than Cu foil current collector in the Mg-DIB. This phenomenon has already demonstrated the key role of carbon paper anode current collector and Cu foam interlayer for the increased specific capacity and stable long-term cycles. Then, to reveal the existence of copper ions in

This article is protected by copyright. All rights reserved.

Author Manuscript

the electrolyte during the electrochemical reaction process, the linear sweep voltammetry (LSV) measurement on the carbon paper electrode was carried out using platinum as the counter electrode, and standard Ag/AgCl electrode as the reference electrode at 5 mV s^{-1} in the electrolyte obtained after CV cycles of the three-electrode cell (working electrode: Cu foam) in $Mg(TFSI)_2$ electrolyte (Figure S12a). After continuous negative scans, red deposits can be clearly seen on the surface of the carbon paper, as shown in Figure S15a. The morphology and component of the carbon paper after the negative scan process were investigated by SEM and XRD (Figure S15b). Metal Cu is covered on the surface of the carbon paper to form a copper film, demonstrating the existence of copper ions and the electrochemical reduction of copper ion to metal Cu during the charge process of the full cell. In-situ formation of metal Cu on the PTCDI electrode improves the electronic conductivity of the organic anode (from 131.03 to 643.97 S mm^{-1}), thus accelerates the promotion of the rate capability and long-term durability of the full cell. In addition, we evaluate the electrochemical performance of the Mg-DIBs full cell using the electrolyte containing both $Cu(TFSI)_2$ and $Mg(TFSI)_2$ without Cu foam interlayer, as shown in Figure S16. The capacity reaches about 142 mAh g^{-1} and remains stable during 100 cycles. However, the capacity decays rapidly after continuing the cycle, which can be ascribed to the limited copper ions in the $Cu(TFSI)_2$+$Mg(TFSI)_2$ electrolyte due to the irreversibility of Cu to Cu^{2+}. The introduction of copper foam interlayer can make the concentration of copper ions in the electrolyte stable and enhance the electronic conductivity of PTCDI electrode via the copper

Author Manuscript

This article is protected by copyright. All rights reserved.

layer on the electrode surface, thus increases the specific capacity and keeps the cycling process stable.

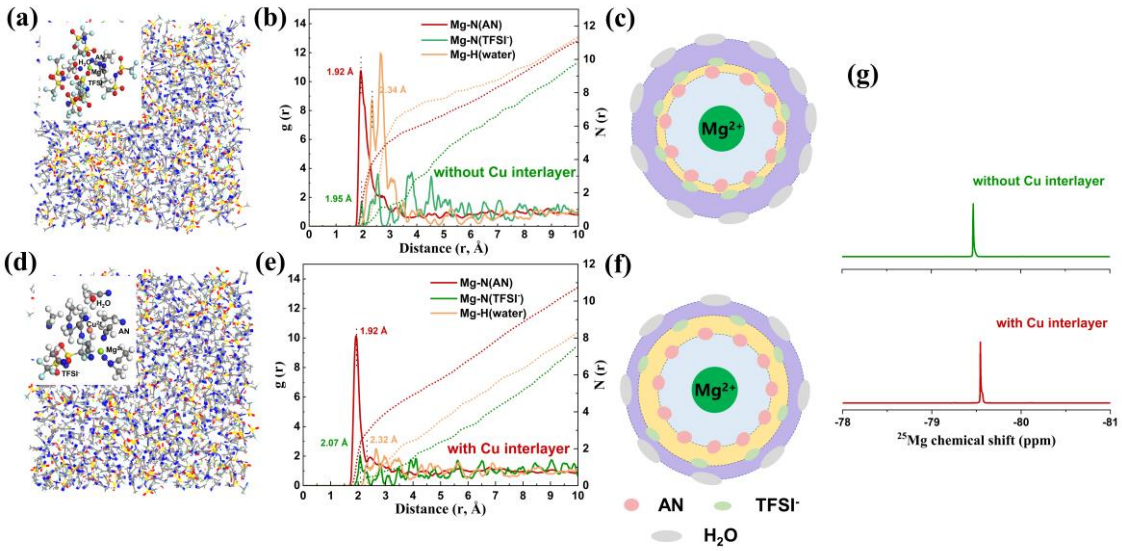

Figure 4. Snapshots of the MD simulation boxes of the $Mg(TFSI)_2$ electrolytes without Cu^{2+} cations (a) and with Cu^{2+} cations (d), insets are the representative solvation structures, colors for different elements: Cu, pink; Mg, light green; S, yellow; F, cyan; N, blue; O, red; H, white; and C, gray; RDFs g(r) (solid lines) and coordination number N (r) (dashed lines) of Mg-N and Mg-H pairs of the electrolytes without Cu^{2+} cations (b) and with Cu^{2+} cations (e). Schematic diagrams of Mg^{2+} representative solvation structures for the electrolytes without Cu^{2+} cations (c) and with Cu^{2+} cations (f). (g) ^{25}Mg NMR of different electrolytes.

Furthermore, to investigate the effect of copper ions to magnesium ions in electrolyte, molecular dynamics (MD) simulations (Figure 4) were carried out to understand the interaction between cations/anions and solvent molecules. The radial distribution function

This article is protected by copyright. All rights reserved.

Author Manuscript

(RDF) $g_{AB}(r)$, referring to the probability of finding another atom at a certain distance, can be used to represent the interaction between two components and evaluate the structures of the pure liquids and their mixtures [26]. According to the radial distribution functions, the Mg-N peak for Mg^{2+} with AN, Mg-N peak for Mg^{2+} with $TFSI^-$, and Mg-H peak for Mg^{2+} with water in the electrolyte without Cu^{2+} cations correspond to the distance of 1.92, 1.95, and 2.34 Å, respectively (Figure 4b). Interestingly, in the electrolyte containing Cu^{2+} cations, the distance of Mg-N peak for Mg^{2+} with $TFSI^-$ shows obvious change away from the centroid Mg^{2+} after Cu incorporation, and a much lower peak intensity of Mg-H peak for Mg^{2+} with water is observed simultaneously (Figure 4e), indicating fewer $TFSI^-$ and H_2O into the Mg^{2+} solvation sheath. The coordination number of Mg^{2+} with AN, H_2O and $TFSI^-$ decreases from 11.12, 11.33, 9.8 to 10.72, 8.3, 7.57 after the addition of Cu foam interlayer in the full cell, respectively. Therefore, Mg^{2+} cations in the electrolyte without Cu^{2+} are more likely to coordinate with solvent and $TFSI^-$ anions than that containing Cu^{2+}, which is consistent with the reduced solvation of Mg^{2+} cations in the electrolyte with Cu interlayer. Moreover, the corresponding 3D schematic diagrams of these two kinds of solvation structures also confirm $TFSI^-$ anions and H_2O move away from the Mg^{2+} cations (Figure 4a, d), which further confirms the solvation of Mg^{2+} cations is weakened. Thus, the calculated results demonstrate that the existence of Cu^{2+} cations significantly reduces the interaction of Mg^{2+} cations with the solvent molecules and $TFSI^-$, making Mg^{2+} cations to react with PTCDI more easily. The variation of Mg^{2+} solvation structure after the addition of Cu foam interlayer was further studied by NMR spectroscopy. A downfield trend of Mg^{2+} peak can be observed in the ^{25}Mg

Author Manuscript

This article is protected by copyright. All rights reserved.

NMR (Figure 4g) from the electrolyte after the addition of Cu foam interlayer, indicating the reduced Mg^{2+}-solvent affinity. Figure 4c, f schematically summarize the solvation structures of Mg^{2+} cations in the electrolytes without and with Cu^{2+} cations, respectively. These findings suggest that more relatively bare Mg^{2+} ions are present in the electrolyte with Cu foam interlayer during the electrochemical process, which further provides extra capacity to the reaction of PTCDI with Mg^{2+} ions.

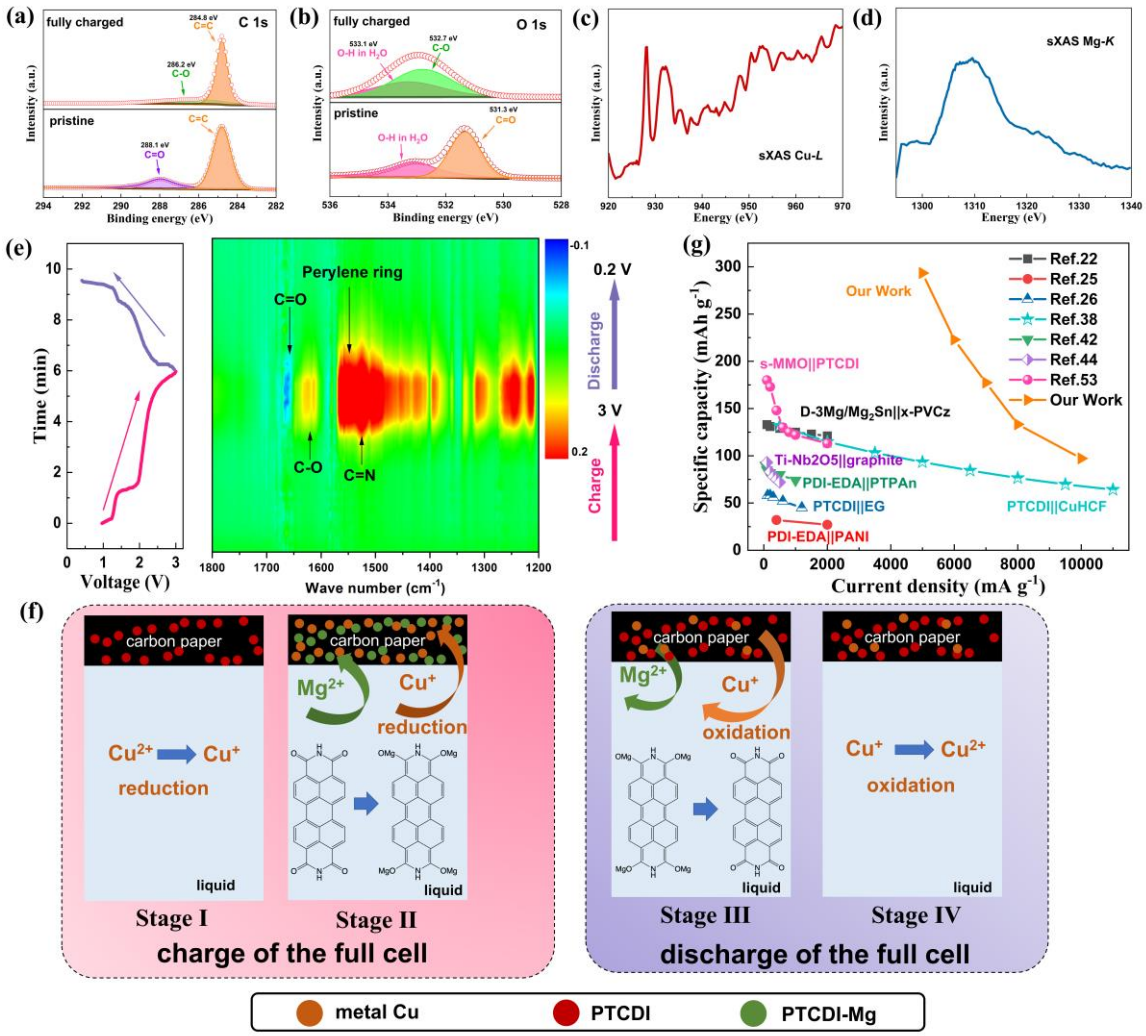

Figure 5. C 1s, O 1s XPS analysis (a-b) of pristine PTCDI and PTCDI anode from fully charged full cell; Cu L-edge (c) and Mg K-edge (d) sXAS spectra of PTCDI anode from fully

This article is protected by copyright. All rights reserved.

charged full cell; In-situ FTIR spectra (e) of the PTCDI anode in the Mg-DIB under different charging/discharging states; (f) the possible electrochemical evolution on anode side and the variation of PTCDI during the charge/discharge processes of EG||PTCDI full cell; (g) Performance comparison between this work and other previously reported Mg-DIBs and MIBs.

In-situ FTIR spectra, ex-situ X-ray photoelectron spectroscopy (XPS) and soft X-ray absorption spectroscopy (sXAS) of the PTCDI anode after fully charged EG||PTCDI full cell were measured for further investigating the specific reaction mechanism of anode side in this Mg-DIB system with Cu foam interlayer. To confirm the break of C=O bonds to form metallic bond during the charge process of the full cell, the PTCDI anode from the fully charged full cell was measured by XPS and the results are illustrated in Figure 5a, b. In C 1s spectra, there exist two peaks at 284.8, 288.1 eV at the pristine state, corresponding to C=C, C=O bonds of PTCDI, respectively. At fully charged state, the characteristic peak of C=O bond weakens, meanwhile a new peak at 286.2 eV related to C-O bond emerges, suggesting the electrochemical reduction of carbonyl groups in PTCDI. In addition, O 1s characteristic peak of C=O bond at 531.3 eV for the pristine state vanishes, and a new peak at 532.7 eV corresponding to C-O bond appears (Figure 5b), which is in agreement with the aforementioned C 1s spectra results. The peak at 533.1 eV is attributed to oxygen of adsorbed H_2O in the outermost layer of the electrode [27]. All peaks of C=O bonds in C 1s and O 1s spectra disappear completely, proving that carbonyl groups in PTCDI completely reacts with Mg^{2+}. This is a key factor in increasing the specific capacity of the full cell. Moreover, we

This article is protected by copyright. All rights reserved.

Author Manuscript

noticed that the intensity of N 1s characteristic peak at 400.0 eV corresponding to the N-H is gradually weakened after full charging (Figure S17), which indicates the formation of hydrogen bond (N-H⋯O-C). Overall these findings are in accordance with previously reported [28]. Figure 5c, d shows the Cu-*L*, Mg-*K* sXAS spectra of the PTCDI anode from fully charged full cell. It is noted that the pristine PTCDI does not contain Cu and Mg element, while the Cu spectrum collected for the anode from the charged full cell shows six intense asymmetric peaks at 928.0, 932.5, 938.0, 942.0, 948.0 and 953.8 eV. The peaks at 932.5, 938.0, 942.0 and 953.8 eV are contributed to the so called L_3 and L_2 excitations of metallic Cu [29]. Those at 928.0 and 948.0 eV correspond to the typical peaks of the Cu^{2+} $L_{2,3}$-edge spectrum [30] due to the partial retention of Cu^{2+} in the fully discharged anode. The Mg-*K* XAS shows an enhanced absorption intensity at 1310.0 eV, which is related to the characteristic of bulk Mg-O [31]. In the O-*K* sXAS of pristine PTCDI (Figure S18), strong features around 532.0 and 535.0 eV arise from the carbonyl group. A probable contribution from CONH is expected in the energy range ~540 eV [32]. After fully charging the cell, the characteristic peaks at 532.0 and ~540 eV weaken and the peak at 535.0 eV vanishes, demonstrating the reduction of the two C=O bonds.

Figure 5e shows the *in-situ* FTIR spectra analysis of the PTCDI anode in the Mg-DIB at different charging/discharging states in the voltage range of 0.2~3.0 V. During charging process of the full cell, the peak at ~1681 cm^{-1} primarily from the carbonyl groups (C=O) gradually weakens and a new peak at ~1608 cm^{-1} originated from the C-O bond gradually strengthens, suggesting the conversion from carbonyl groups (C=O) to enolate groups (C-O).

This article is protected by copyright. All rights reserved.

Author Manuscript

In addition, the reduction of the C=O bonds leads to a decreased π-conjugation in the PTCDI structure, as reflected by strengthened stretching vibrations of perylene ring and C=N from 1574 to 1500 cm^{-1}. Upon discharging process, all the above peaks recover to their original positions and intensities, revealing good reversibility of Mg insertion/extraction.

Based on these results, the Mg-ion storage mechanism of PTCDI in the Mg-DIB containing Cu foam interlayer is clear and largely dominated by gaining/losing electrons from the oxidation/reduction state of the organic conjugated moiety (C=O groups) and copper ion. The possible electrochemical evolution at PTCDI anode side during the charging/discharging of the full cell is as follows (Figure 5f): *Charge:* Stage I, the reduction of Cu(II) → Cu(I); Stage II, the reduction of the carbonyl groups with Mg^{2+} in PTCDI and Cu(I) → Cu(0); *Discharge:* Stage III, the oxidation of PTCDI-Mg to form the carbonyl groups and Cu(0) → Cu(I); Stage IV, the oxidation of Cu(I) → Cu(II). A comparison with the electrochemical performance of Mg-DIBs [12, 15-16, 24, 28] and MIBs [33] summarized in Figure 5g highlights the excellence of Mg-DIBs with Cu foam interlayer in this work. Our work introduces the copper ions into MIBs for the first time, enhances the deep understanding of copper ion in MIBs, and provides guidance for the development of dynamic ion redox towards high energy density of MIBs.

3. Conclusions

In this work, with a novel aqueous/organic hybrid electrolyte and a Cu foam interlayer between the anode and the separator, the MIB containing a PTCDI anode and a EG cathode realizes an ultra-high capacity (205 mAh g^{-1}, 243 Wh kg^{-1} at a current density of 5 A g^{-1}),

This article is protected by copyright. All rights reserved.

Author Manuscript

4-fold higher than those in conventional organic or aqueous electrolytes, as well as excellent cycling stability after 600 cycles and rate capability (138 mAh g^{-1}, 81 Wh kg^{-1} at 10 A g^{-1}). Through first-principles calculations and in-situ/ex-situ characterizations, we found that the Mg-ion storage in PTCDI anode is dominated by gaining/losing electrons from the oxidation/reduction state of the organic conjugated moiety. The dynamic redox of copper ions, the weakened solvation of Mg^{2+} cations in the electrolyte and the enhanced electronic conductivity of anode offer effective capacity-compensation to the PTCDI-Mg conversion reactions during long-term cycles. These meaningful findings will provide a new avenue for the rational design of MIBs with a high energy density and a low cost.

Experimental Section

Preparation of electrodes：3,4,9,10-perylenetetracarboxylic acid diimide (PTCDI) anode was fabricated through grinding PTCDI powder (Meryer Chemical Technology Co., Ltd, > 95.0%), carbon black (Super P) and polyvinylidene fluoride (PVDF) with a weight ratio of 7:2:1 in N-methyl-2-pyrrolidone (NMP) solvent to form a uniform slurry, and coating uniformly onto carbon paper (Toray) and drying at 80 °C under vacuum for 12 h. The expand graphite (EG) cathode was prepared by grinding EG powder (3Achem, particle size of 50 μm), Super P, and PVDF with a ratio of 8:1:1 in the NMP solvent to form a homogeneous slurry. The slurry was coated onto carbon paper and dried at 80 °C in vacuum for 12 h. Each

Author Manuscript

This article is protected by copyright. All rights reserved.

cathode electrode contained active material with a mass loading of ca. 2.0 mg cm^{-2}. The mass loading ratio of cathode to anode was ca. 10:1.

Preparation of the electrolytes: 1 mol L^{-1} $Mg(TFSI)_2$ electrolytes in the organic, aqueous or hybrid solvents of acetonitrile (AN)/H_2O were achieved through adding the predetermined amount $Mg(TFSI)_2$ (Huizhou Dado New Material Technology Co., Ltd, 99.5%) in AN (Aladdin), deionized water or AN/deionized water at the fixed volume ratios (4.9:0.1, 4.7:0.3, 4.5:0.5 and 4.0:1.0) under stirring for full dissolution in air, respectively. The $Cu(TFSI)_2$ electrolyte was prepared by adding 49.9 mg $Cu(TFSI)_2$ (Aladdin) into 2 mL AN/deionized water (4.9:0.1 volume ratio).The $Cu(TFSI)_2$+$Mg(TFSI)_2$ electrolyte was prepared by adding 49.9 mg $Cu(TFSI)_2$, 1.1692 g $Mg(TFSI)_2$ into 2 mL AN/deionized water (4.9:0.1 volume ratio).

Characterization: X-ray diffraction (XRD) measurements with Cu Kα radiation were performed on a D/MAX-2200/PC Rigaku diffractometer. Scanning electron microscopy (SEM) used a JSM-7401F field-emission microscope, and high-angle annular dark field scanning transmission electron microscopy (HAADF-STEM) with energy-dispersive x-ray spectroscopy (EDS) was taken on a TALOS F200X microscope. Information on the functional groups of imidazole PTCDI has been obtained by a Fourier Transform Infrared Spectroscope (FTIR, NICOLE6700). X-ray photoelectron spectroscopy (XPS) analysis was conducted on an AXIS Ultra DLD with 284.8 eV C 1s line and monochromatic Al Kα radiation. The soft X-ray absorption spectroscopy (sXAS) measurements were carried out on

This article is protected by copyright. All rights reserved.

Author Manuscript

the BL08U1A beamline at Shanghai Synchrotron Radiation Facility (SSRF). The electronic conductivity measurement of the PTCDI electrodes with carbon paper was performed using a four-point probe tester (FT-371, Ningbo Rooko Instrument Co., Ltd.)

Electrochemical Measurements: CR2032 coin cells with a EG cathode, a glass fiber separator, a Cu foam interlayer, a PTCDI anode, and 1 mol L^{-1} $Mg(TFSI)_2$ in AN/H_2O electrolyte were assembled in air. Galvanostatic cycling and rate measurements were carried out with a 0.2~3.0 V cut-off voltage range on a Land battery test system. Cyclic voltammograms (CVs) were conducted on a CHI650C electrochemical workstation (CH Instruments Inc., Shanghai). The ionic conductivity of the electrolytes was measured by a conductivity instrument (DDS-307A).

Calculation methods: In this work, DFT calculations of PTCDI-Cu were carried out by utilizing the projector augmented wave (PAW) method [34] implemented in the Vienna ab initio simulation package (VASP) [35]. The exchange-correlation function is described by the generalized gradient approximation (GGA) [36] with Perdew-Burke-Ernzerhof (PBE) approach [37] with an energy cut-off of 480 eV. The convergence criteria of energy was set to be 10^{-5} eV and a $6\times2\times3$ Gamma centered k-mesh was adopted. During the process of geometric optimization for the PTCDI and PTCDI-Cu systems, cell parameters, cell shape, and atomic coordinates were free to change.

Molecular dynamics (MD) simulations were carried out by using the Forcite module with COMPASS force field for 1 mol L^{-1} $Mg(TFSI)_2$ with solvent molecules (AN and H_2O), and

This article is protected by copyright. All rights reserved.

Author Manuscript

the simulation box size was 40.6×40.6×40.6 Å. Cu^{2+} model contains 50 Mg^{2+}, 50 Cu^{2+}, 100 $TFSI^-$, 938 AN and 56 H_2O. Properties such as the radial distribution function (RDF) were obtained with the NVT ensemble at a volume determined by the NVE and NPH simulation. The temperature and the pressure were maintained at 298 K and 10^{-4} GPa, the time step and the total simulation time were 1 fs and 100 ps, and the number of steps was 5000 in NVT.

Supporting Information

The Supporting Information is available free from the Wiley Online Library or the author.

Acknowledgments

We greatly acknowledge the financial support from the National Natural Science Foundation of China (No. 21975159, 21573146, U1705255), Open Fund of Shanghai Jiao Tong University Shaoxing Institute of New Energy and Molecular Engineering (No, JDSX2022033), Oceanic Interdisciplinary Program of Shanghai Jiao Tong University (No. WH410260401/006). We thank the Supercomputing Center of the Dalian University of Technology for providing computing resources. The work was also carried out at Shanxi Supercomputing Center of China, and the calculations were performed on TianHe-2.

Received: ((will be filled in by the editorial staff))

Revised: ((will be filled in by the editorial staff))

Published online: ((will be filled in by the editorial staff))

Conflict of Interest

This article is protected by copyright. All rights reserved.

Author Manuscript

The authors declare no competing financial interest.

REFERENCES

[1] a) N. Nitta, F. Wu, J. T. Lee, G. Yushin, *Mater. Today* **2015**, 18, 252; b) J. M. Tarascon, M. Armand, *Nature* **2001**, 414, 359.

[2] S. Yang, F. Zhang, H. Ding, P. He, H. Zhou, *Joule* **2018**, 2, 1648.

[3] C. Xu, Q. Dai, L. Gaines, M. Hu, A. Tukker, B. Steubing, *Commun. Mater.* **2020**, 1, 99.

[4] P. Sun, R. Bisschop, H. Niu, X. Huang, *Fire Technol.* **2020**, 56, 1361.

[5] a) A. Ponrouch, J. Bitenc, R. Dominko, N. Lindahl, P. Johansson, M. R. Palacin, *Energy Storage Mater.* **2019**, 20, 253; b) P. Canepa, G. Sai Gautam, D. C. Hannah, R. Malik, M. Liu, K. G. Gallagher, K. A. Persson, G. Ceder, *Chem. Rev.* **2017**, 117, 4287; c) Y. Liang, H. Dong, D. Aurbach, Y. Yao, *Nat. Energy* **2020**, 5, 646.

[6] a) L. Yin, B. J. Kwon, Y. Choi, C. J. Bartel, M. Yang, C. Liao, B. Key, G. Ceder, S. H. Lapidus, *J. Am. Chem. Soc.* **2021**, 143, 10649; b) F. Xiong, Y. Jiang, L. Cheng, R. Yu, S. Tan, C. Tang, C. Zuo, Q. An, Y. Zhao, J.-J. Gaumet, L. Mai, *Interdiscip. Mater.* **2022**, 1, 140.

[7] J. Li, C. Han, X. Ou, Y. Tang, *Angew. Chem. Int. Ed.* **2022**, 61, e202116668.

[8] Y. Zhang, B. Zhang, J. Li, J. Liu, X. Huo, F. Kang, *Chem. Eng. J.* **2021**, 403, 126377.

[9] D. Wu, W. Ren, Y. NuLi, J. Yang, J. Wang, *J. Mater. Sci. Technol.* **2021**, 91, 168.

[10] a) Z. Zhao-Karger, R. Liu, W. Dai, Z. Li, T. Diemant, B. P. Vinayan, C. Bonatto Minella, X. Yu, A. Manthiram, R. J. Behm, M. Ruben, M. Fichtner, *ACS Energy Lett.* **2018**, 3, 2005; b) J. Luo, S. He, T. L. Liu, *ACS Energy Lett.* **2017**, 2, 1197; c) H. S. Kim, T. S. Arthur, G. D. Allred, J. Zajicek, J. G. Newman, A. E. Rodnyansky, A. G. Oliver, W. C. Boggess, J. Muldoon, *Nat. Commun.* **2011**, 2, 427; d) O. Mizrahi, N. Amir, E. Pollak, O. Chusid, V. Marks, H. Gottlieb, L. Larush, E. Zinigrad, D. Aurbach, *J. Electrochem. Soc.* **2008**, 155, A103; e) W. Ren, D. Wu, Y. N. NuLi, D. Zhang, Y. Yang, Y. Wang, J. Yang, J. L. Wang, *ACS Energy Lett.* **2021**, 6, 3212; f) Y. Yang, Y. Qiu, Y. NuLi, W. Wang, J. Yang, J. Wang, *J. Mater. Chem. A* **2019**, 7,

Author Manuscript

This article is protected by copyright. All rights reserved.

18295; g) W. Ren, D. Wu, Y. NuLi, X. Zhang, J. Yang, J. Wang, *ACS Appl. Mater. Interfaces* **2021**, 13, 32957.

[11] a) P. Saha, M. K. Datta, O. I. Velikokhatnyi, A. Manivannan, D. Alman, P. N. Kumta, *Prog. Mater Sci.* **2014**, 66, 1; b) E. Levi, Y. Gofer, D. Aurbach, *Chem. Mater.* **2010**, 22, 860.

[12] A. B. Ikhe, J. Y. Seo, W. B. Park, J.-W. Lee, K.-S. Sohn, M. Pyo, *J. Power Sources* **2021**, 506, 230261.

[13] M. Wang, Y. Tang, *Adv. Energy Mater.* **2018**, 8, 1703320.

[14] P. Seggem, S. N. Chavan, S. Biswas, V. R. Jetti, *ACS Appl. Energy Mater.* **2021**, 4, 5165.

[15] R. Yang, F. Zhang, X. Lei, Y. Zheng, G. Zhao, Y. Tang, C.-S. Lee, *ACS Appl. Mater. Interfaces* **2020**, 12, 47539.

[16] D. Lu, H. Liu, T. Huang, Z. Xu, L. Ma, P. Yang, P. Qiang, F. Zhang, D. Wu, *J. Mater. Chem. A* **2018**, 6, 17297.

[17] a) Y. Zhang, P. Nie, C. Xu, G. Xu, B. Ding, H. Dou, X. Zhang, *Electrochim. Acta* **2018**, 268, 512; b) M. Pasta, C. D. Wessells, R. A. Huggins, Y. Cui, *Nat. Commun.* **2012**, 3, 1149; c) Y. Xu, Z. C. Liu, X. H. Zheng, K. Li, M. M. Wang, W. Yu, H. L. Hu, W. Chen, *Adv. Energy Mater.* **2022**, 12, 2103352.

[18] a) J. Song, M. Noked, E. Gillette, J. Duay, G. Rubloff, S. B. Lee, *Phys. Chem. Chem. Phys.* **2015**, 17, 5256; b) Y. Zhu, X. Guo, Y. Lei, W. Wang, A.-H. Emwas, Y. Yuan, Y. He, H. N. Alshareef, *Energy Environ. Sci.* **2022**, 15, 1282; c) Y. Tang, X. Li, H. Lv, W. Wang, Q. Yang, C. Zhi, H. Li, *Angew. Chem. Int. Ed.* **2021**, 60, 5443.

[19] a) S. Zhang, Y. Huang, Y. NuLi, B. Wang, J. Yang, J. Wang, *J. Phys. Chem. C* **2020**, 124, 20712; b) S. Zhang, W. Ren, Y. NuLi, B. Wang, J. Yang, J. Wang, *Chem. Eng. J.* **2022**, 427, 130902; c) L. Zeng, N. Wang, J. Yang, J. Wang, Y. NuLi, *J. Electrochem. Soc.* **2017**, 164, A2504; d) A. B. Du, Y. M. Zhao, Z. H. Zhang, S. M. Dong, Z. L. Cui, K. Tang, C. L. Lu, P. X. Han, X. H. Zhou, G. L. Cui, *Energy Storage Mater.* **2020**, 26, 23.

[20] a) P. He, H. O. Ford, L. C. Merrill, J. L. Schaefer, *ACS Appl. Energy Mater.* **2019**, 2, 6800; b) A. Robba, M. Mežnar, A. Vizintin, J. Bitenc, J. Bobnar, I. Arčon, A. Randon-Vitanova, R. Dominko, *J. Power Sources* **2020**, 450, 227672.

Author Manuscript

This article is protected by copyright. All rights reserved.

[21] M. Shimizu, A. Nakahigashi, S. Arai, *Phys. Chem. Chem. Phys.* **2021**, 23, 16981.

[22] a) K. Beltrop, P. Meister, S. Klein, A. Heckmann, M. Grünebaum, H.-D. Wiemhöfer, M. Winter, T. Placke, *Electrochim. Acta* **2016**, 209, 44; b) Z. Huang, Y. Hou, T. Wang, Y. Zhao, G. Liang, X. Li, Y. Guo, Q. Yang, Z. Chen, Q. Li, L. Ma, J. Fan, C. Zhi, *Nat. Commun.* **2021**, 12, 3106.

[23] H. Li, T. Kurihara, D. Yang, M. Watanabe, T. Ishihara, *Energy Storage Mater.* **2021**, 38, 454.

[24] Y. Zhu, J. Yin, A. H. Emwas, O. F. Mohammed, H. N. Alshareef, *Adv. Funct. Mater.* **2021**, 31, 2107523.

[25] C. Rousse, S. Beaufils, P. Fricoteaux, *Electrochim. Acta* **2013**, 107, 624.

[26] H. Takaba, W. Yamamoto, M. K. Alam, *Bangladesh J. Phys.* **2020**, 27, 13.

[27] B. Peng, T. Song, T. Wang, L. Chai, W. Yang, X. Li, C. Li, H. Wang, *Chem. Eng. J.* **2016**, 299, 15.

[28] X. Lei, Y. Zheng, F. Zhang, Y. Wang, Y. Tang, *Energy Storage Mater.* **2020**, 30, 34.

[29] F. Tavani, M. Fracchia, A. Tofoni, L. Braglia, A. Jouve, S. Morandi, M. Manzoli, P. Torelli, P. Ghigna, P. D'Angelo, *Phys. Chem. Chem. Phys.* **2021**, DOI: 10.1039/D1CP03946F.

[30] R. Wang, X. Li, X. Han, J. Lin, Y. Wang, T. Qian, H. Ding, Y. Shi, X. Liu, *Chin. Phys. B* **2021**, 30, 046102.

[31] L. F. Wan, Y.-S. Liu, E. S. Cho, J. D. Forster, S. Jeong, H.-T. Wang, J. J. Urban, J. Guo, D. Prendergast, *Nano Lett.* **2017**, 17, 5540.

[32] F. Frati, M. O. J. Y. Hunault, F. M. F. de Groot, *Chem. Rev.* **2020**, 120, 4056.

[33] a) Z. Zhang, Y. Li, G. Zhao, L. Zhu, Y. Sun, F. Besenbacher, M. Yu, *ACS Appl. Mater. Interfaces* **2021**, 13, 40451; b) B. Wen, C. Yang, J. Wu, J. Liu, W. Wang, J. Yang, X. Chi, Y. Liu, *Chem. Eng. J.* **2022**, 435, 134997.

[34] P. E. Blöchl, *Physical review B* **1994**, 50, 17953.

[35] J. Hafner, *J. Comput. Chem.* **2008**, 29, 2044.

[36] J. P. Perdew, W. Yue, *Physical review B* **1986**, 33, 8800.

Author Manuscript

This article is protected by copyright. All rights reserved.

[37] W. Kohn, L. J. Sham, *Physical review* **1965**, 140, A1133.

Author Manuscript

Table of content

The assembled unusual MIBs using expanded graphite (EG) cathode coupled with 3,4,9,10-perylenetetracarboxylic diimide (PTCDI) anode in a novel hybrid aqueous/organic electrolyte achieve an ultra-high capacity (205 mAh g^{-1}, 243 Wh kg^{-1} at 5 A g^{-1}) as well as unprecedented cycling stability after 600 cycles and rate capability (138 mAh g^{-1}, 81 Wh kg^{-1} at 10 A g^{-1}). The introduction of Cu foam interlayer between anode and separator offer effective capacity-compensation during long-term cycles by means of the dynamic redox of copper ions, the weakened solvation of Mg^{2+} cations and the enhanced electronic conductivity of anode. Such excellent electrochemical performance would lead to low-cost and high-performance Mg-ion batteries for potential industrialization in electric vehicles or energy storage power stations.

Shuxin Zhang, Yaowei Wang, Yukun Sun, Yaru Wang, Yang Yang, Peng Zhang, Xuecheng Lv, Jiulin Wang, Hong Zhu, Yanna NuLi*

This article is protected by copyright. All rights reserved.

High-energy aqueous magnesium ion batteries with capacity-compensation evolved from dynamic copper ion redox

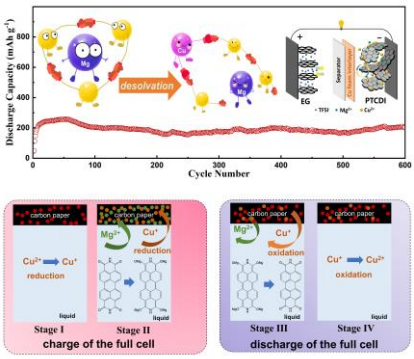

Author Manuscript

This article is protected by copyright. All rights reserved.